A 1-bit reconfigurable intelligent metasurface-based antenna design for 5G application

Yajun Zhou, Lianfeng Chen, Qifei Zhang, Hao Wang and Linyan Guo [ID]

School of Geophysics and Information Technology, China University of Geosciences, Beijing, China

Abstract

A 1-bit reconfigurable intelligent metasurface-based antenna for 5G application is proposed. The proposed antenna based on artificial electromagnetic metamaterial has the advantages of easy processing and low cost. This meets the requirements of future communication network development. This antenna shows that the unit cell has a stable 180° phase difference between the ON and OFF states by loading a PIN diode at 6.425–7.125 GHz. A 10×10 array antenna is constructed by using 2×2 meta-atoms to reduce the complexity of the control network. This proposed antenna can achieve $\pm 40°$ beam scanning with a gain tolerance of 3 dB and a maximum gain of 18.7 dBi. In addition, beamforming performance, such as multi-beams, is also achieved. These properties ensure that the proposed antenna has great potential in wireless communication systems and microwave imaging systems.

Introduction

With the rapid development of wireless communication and the popularization of smart devices, the volume of communication data and the number of connections have shown explosive growth. In the fifth-generation (5G) wireless networks, high spectrum efficiency, low latency, and low energy consumption will all be the key research directions. Due to the complex feed network and high power consumption of traditional phased array antennas and the multi-base station deployment scheme of future communication systems, the potential of massive multiple-input multiple-output technology cannot be fully realized.

According to the future wireless communication scheme, a low-energy, small-sized, and low-cost equipment is required to realize the relay function. Reconfigurable intelligent surface (RIS) is a promising technique alternative to the traditional phased arrays [1–5]. Based on a special periodic structure of artificial electromagnetic metamaterials, RIS is mainly composed of a large number of passive components with ultralow power consumption [6–17]. Relying on the special electromagnetic properties of metamaterials, phase control of the incident wave is performed on each unit cell to achieve specific functions, such as focusing [6, 7], beamforming [8, 9], polarization conversion [10, 11], perfect absorption [12–14], abnormal reflection [15], RCS reduction [16, 17], and so on. The RIS-based antenna has been developed rapidly in recent years due to its advantages of low profile, lightweight, high gain, low cost, and easy integration. It can be used in many fields such as satellite, radar, and wireless communication and is expected to become a promising infrastructure in future wireless communication.

In order to make the antennas more suitable for reconfigurable characteristics, some researchers have proposed to load active controllable components in RIS, such as PIN diodes or Micro-Electro-Mechanical-Systems [18–23], to meet the needs of complex and changeable scenarios. Thus, RIS is also known as the coding metamaterials. In Dai et al. [24], the prototype of a wireless communication system based on RIS was designed for the first time, and the experimental evaluation proved for the first time the feasibility and efficiency of energy-saving wireless communication by using RIS instead of the traditional phased array.

In response to high communication rate requirements, measures have been taken to broaden the communication frequency spectrum. Under China's strong promotion, the 2023 World Radiocommunication Conference (WRC-23) agenda 1.2 decided to consider the identification of the frequency band 6425–7125 MHz for International Mobile Telecommunications (IMT), including possible allocations to the mobile service on a primary basis in accordance with Resolution 245 (WRC-19) [25]. This frequency band is expected to become a new frequency band of the IMT (5G or 6G in the future), further expanding spectrum resources. Currently, the design of RIS-based antenna is mainly concentrated in the low frequency [24] and millimetre-wave [10, 11, 14], and the research on this new application band has great application prospects.
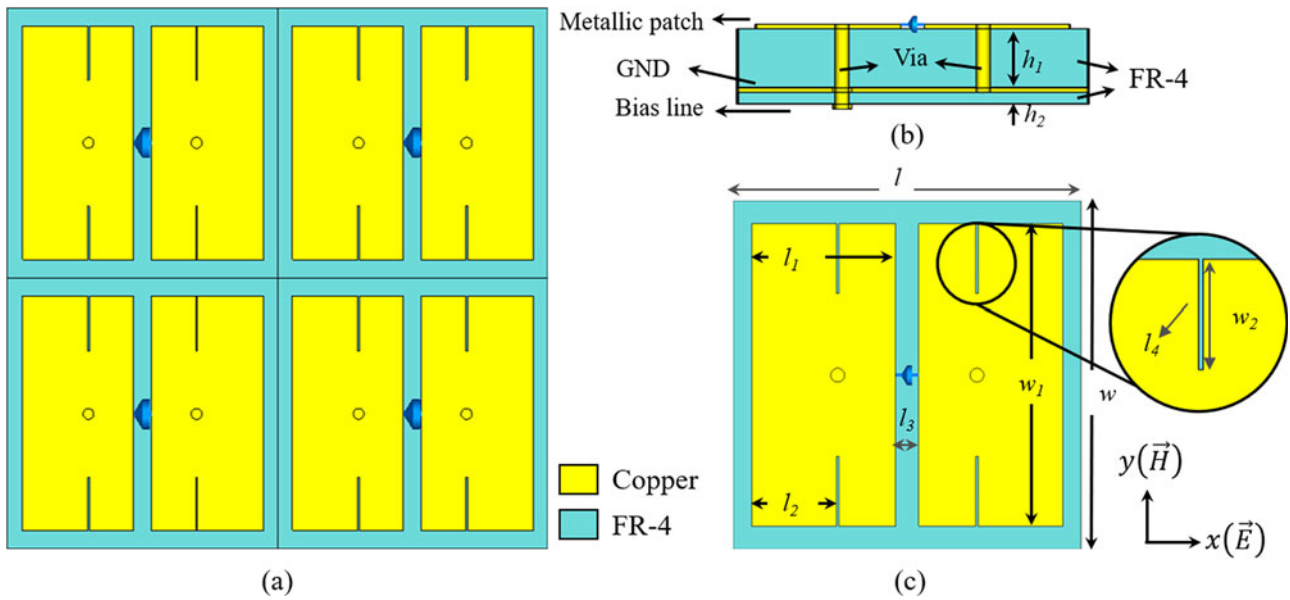
Figure 1. The configuration of the unit cell: (a) unit cell, (b) meta-atom on the side view, and (c) meta-atom on the top view.
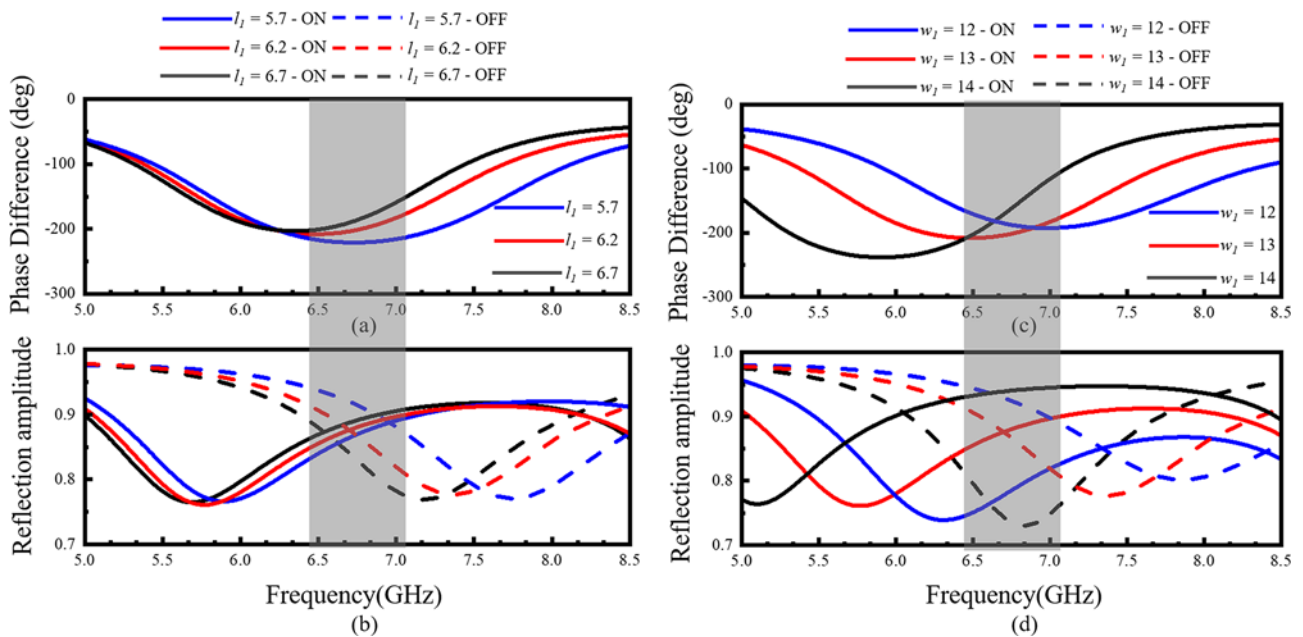

Figure 2. Scattering parameters of meta-atoms with the PIN diode ON/OFF state. For l_1, (a) phase difference and (b) reflection amplitude. For w_1, (c) phase difference and (d) reflection amplitude.

Therefore, this paper proposes an RIS-based antenna in the frequency band proposed in WRC-19. The proposed unit cell keeps a stable phase difference between the ON/OFF two states by controlling the voltage of the loaded PIN diode. Meanwhile, the proposed antenna utilizes composite unit cells to reduce the complexity of control and production costs. By modifying the distribution of unit cells, it can achieve $\pm 40°$ beam scanning. In addition, it can also implement multi-beam effects for calculating imaging and multi-receiver communications.

Design of RIS with 1-bit unit cell

As a reflective RIS, it should ensure reflective efficiency when designing the unit cell structure. In order to realize the reconfigurable function, it is necessary to provide a stable 180° phase difference between ON/OFF states. In this 1-bit metamaterial design, the switching diode element is selected to adjust the reflection phase difference, so this element needs to be designed at the unit's peak value of the surface current. The proposed 1-bit RIS-based unit cell is shown in Fig. 1. In order to achieve a good reflection effect and prevent electromagnetic energy leakage, an RIS-based antenna generally consists of hundreds of unit cells. It leads to an increase in the number and complexity of biasing lines. Therefore, considering the size of the unit cell is too small for the half wavelength at the center frequency of 6.8 GHz ($\lambda_0 = 44$ mm), each unit cell consists of 2×2 identical meta-atoms as shown in Fig. 1(a). It can avoid the complexity of circuit control and expensive manufacturing costs, although the accuracy of the

reflection beam is slightly reduced. At the same time, the grating lobes can be avoided by increasing the unit interval.

As shown in Fig. 1(b), the meta-atom consists of two symmetrical rectangular patches ($w_1 \times l_1$) loaded on the top side and bias lines on the opposite side. The patches and bias lines are printed on two identical substrates (FR-4, $\varepsilon_r = 4.3$, $\tan \delta = 0.025$, $h_1 = 2.5$ mm, $h_2 = 0.5$ mm) separated by a copper ground plane. One of the patches is connected with the bias lines by a metalized via hole. The thickness of the copper is 0.03 mm and the conductivity is $\sigma = 5.96 \times 10^7$ S/m. Moreover, the other patch is connected with the ground plane by another metalized via. The radius of all the via holes is 0.5 mm.

Figure 1(c) shows that the PIN diode connecting the two symmetrical metal patches is located in the middle of the y-axis. In the top layer, the metallized patches have four slots, which are used to enhance resonance. Moreover, two metallized patches are connected to the ground plane and the bias lines through two vias, respectively. So, the voltage between the PIN diode can be controlled by the bias lines.

The control variable method is used to optimize each dimension of the meta-atom by the parameter sweep function in Computer

Figure 3. The equivalent circuit of the PIN diode: (a) ON state and (b) OFF state.

Simulation Technology (CST) Studio Suite. Scattering characteristics of meta-atoms in the PIN diode ON/OFF state with different sizes are shown in Fig. 2. It can be seen that the lengths l_1 and w_1 of the metal patches affect the working frequency band. When the target frequency is selected at 6.425–7.125 GHz, the final lengths of the patches are $l_1 = 6.2$ mm and $w_1 = 13$ mm. Other parameters in the element are optimized by similar methods. The geometrical parameters of the meta-atom are given as $l = 15$ mm, $l_2 = 3.65$ mm, $l_3 = 1$ mm, $l_4 = 0.1$ mm, $w = 15$ mm, $w_2 = 3$ mm.

Considering various factors, SKYWORKS's PIN diode, SMP1340-040LF, is selected as the key component of realizing the reconfigurable functions because of its broad frequency band and low insertion loss. According to the datasheet provided by SKYWORKS, a diode can be modeled as an RLC equivalent circuit, as shown in Fig. 3. According to the element scattering parameter file provided by SKYWORKS, the specific equivalent parameters of its ON/OFF states in the working frequency are obtained by using the parameter fitting method in Advanced Design System. In numerical simulations, the ON/OFF states of the PIN diode are represented by effective circuits displayed in Fig. 3. In the ON state, the real equivalent circuit is a series RLC circuit with a capacitance of $C_{ON} = 1.6 \times 10^{-13}$ F, an inductance of $L_{ON} = 0.45 \times 10^{-9}$ H, and a resistance of $R_{ON} = 10$ Ω. In the OFF state, it is a series RL circuit with an inductance of $L_{OFF} = 0.45 \times 10^{-9}$ H and a resistance of $R_{OFF} = 1$ Ω.

The proposed meta-atom and unit cell are analyzed using periodic boundary by the full-wave simulation CST Microwave Studio. The unit cell conditions are set in the y- and x-directions. The perfect electric ($E_t = 0$) is set as the full ground in $-z$. The excitation source is the plane wave, which propagates in the z-direction, and the frequency-domain solver with a tetrahedral mesh is utilized for simulation. Figure 4(a) shows that the reflection phase difference of both the unit cell and the meta-atom between the ON/OFF state is 180° ($\pm 20°$), and the reflection amplitude is more than 0.75 at the working frequency band. These indicate that the proposed element meets the requirement of RIS.
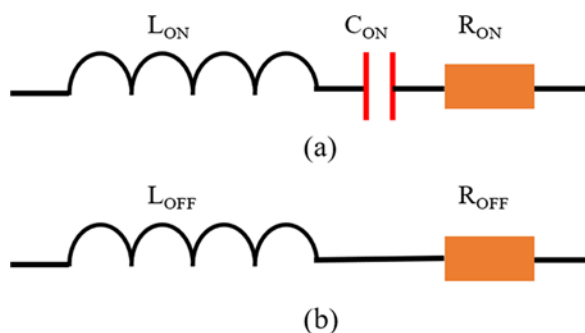

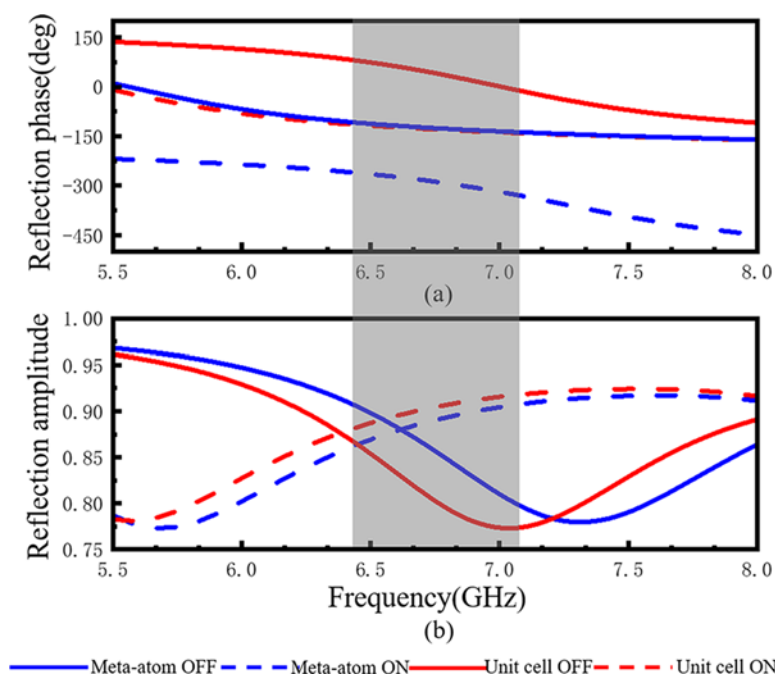**Figure 4.** Reflection parameters of the meta-atom and the unit cell: (a) phase and (b) amplitude.
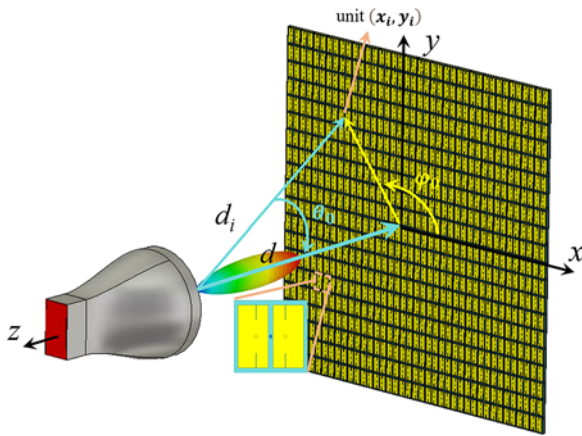
Figure 5. The prototype of RIS-based antenna.

RIS-based antenna

Figure 5 shows the proposed RIS-based antenna prototype. Based on the proposed 2 × 2 meta-atoms, the size of a 10 × 10 RIS prototype is 300 mm × 300 mm × 3.1 mm. Referring to related research about RIS in wireless communication [4,5], the horn antenna is chosen as feed in this design. It has higher directivity and gain than other antennas. Besides, it also has a better time-domain characteristic such as lower tailing, which reduces signal noise interference.

In traditional RIS designs, the object is placed in the far-field region of the feed to obtain better radiation performance. The aperture efficiency or gain can be optimized by properly choosing the feed location to balance the spillover efficiency and illumination efficiency [26]. The ratio of the feed distance and the maximum length of RIS increases, with the directivity of the feed antenna being better. High aperture efficiency is able to be acquired with a narrow beamwidth feed but at the cost of a large reflectarray antenna profile [27]. When the feed distance is shortened, the aperture efficiency of the feed antenna decreases and the beam width increases. When the feed distance is too short, it is necessary to correct the phase of the feed radiation. As the feed distance increases, the risk of radiation leakage increases and requires improved feed antenna performance. The ratio of the feed distance and the maximum length of RIS ranges between 0.7 and 1.0, which can provide a good aperture efficiency with a manageable reflectarray antenna profile. Therefore, this design chooses $d = 300$ mm as the distance between RIS and the feed antenna, in which the ratio is 1.

Suppose that the incident wave reaches the ith unit and radiates again to produce a reflected main beam in the direction of (θ_0, φ_0). According to the theory of array synthesis, the phase shift of the reflective unit can be expressed as

$$\phi(x_i, y_i) = -k_0 (x_i \sin\theta_0 \cos\varphi_0 + y_i \sin\theta_0 \sin\varphi_0). \quad (1)$$

Here, k_0 is the propagation constant of electromagnetic waves in a vacuum and (x_i, y_i) is the coordinate of the ith unit.

The compensation phase quantity $\phi_R(x_i, y_i)$ of the ith unit can be calculated as

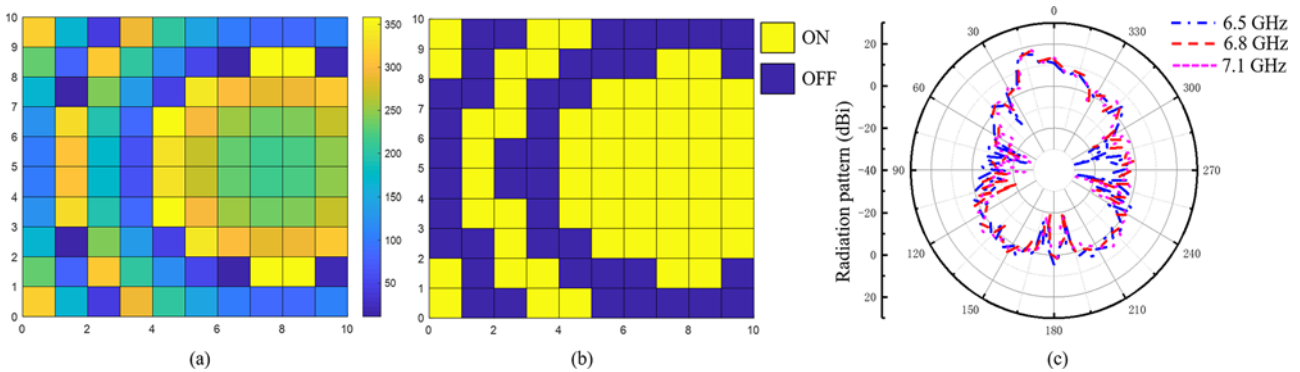$$\phi_R(x_i, y_i) = \frac{2\pi c}{f} (d_i - (x_i \cos\varphi_0 + y_i \sin\varphi_0) \sin\theta_0), \quad (2)$$

Figure 6. (a) Phase continuous distribution, (b) phase discrete distribution, and (c) simulation pattern at 15°.
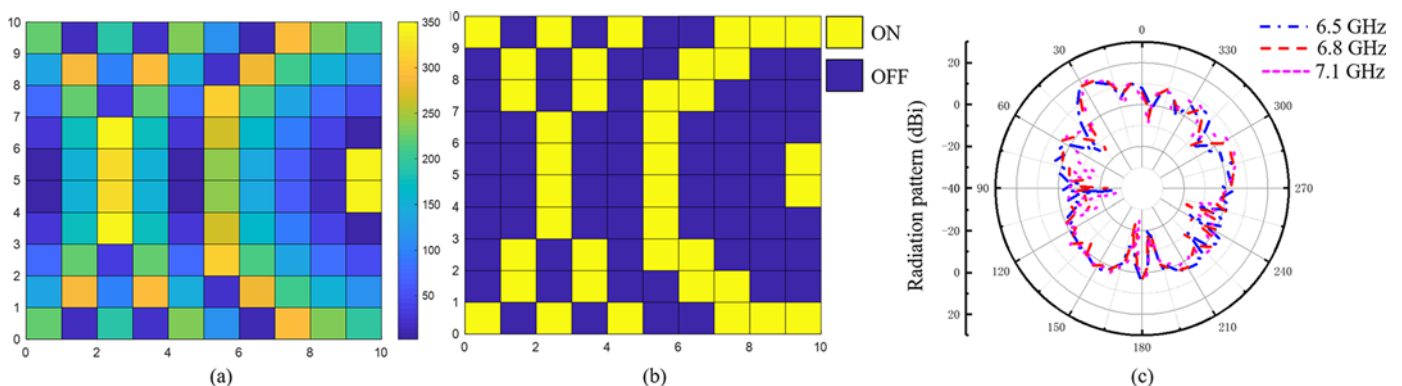

Figure 7. (a) Phase continuous distribution, (b) phase discrete distribution, and (c) simulation pattern at 30°.
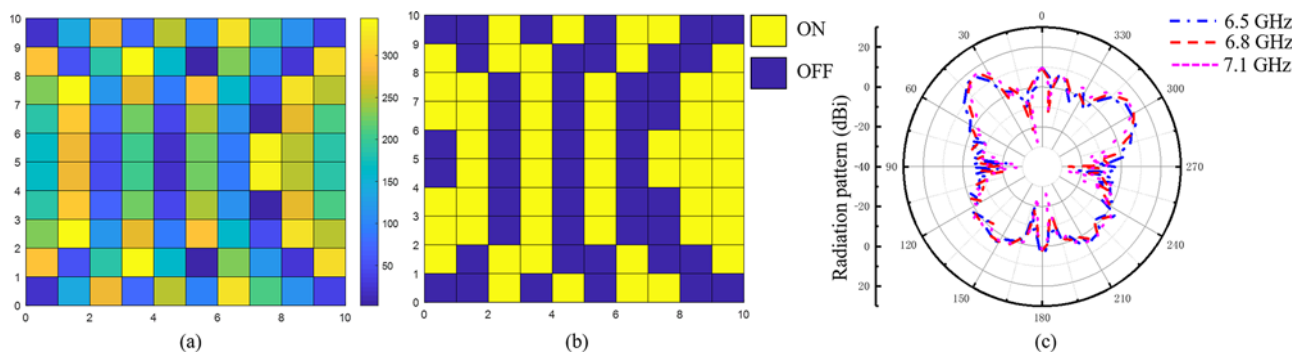
Figure 8. (a) Phase continuous distribution, (b) phase discrete distribution, and (c) simulation pattern at 40°.
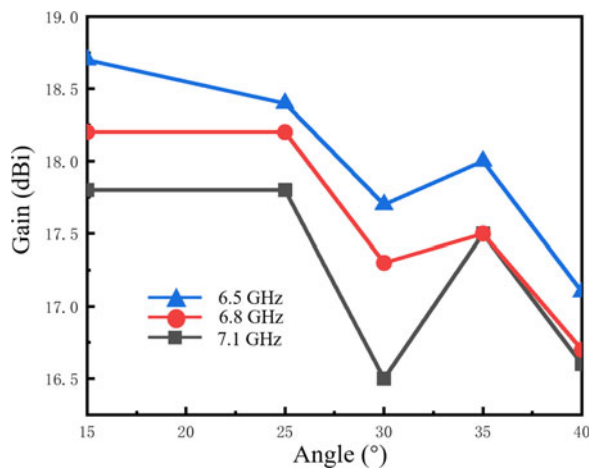

Figure 9. Simulated gains at different scan angles at 6.5 GHz, 6.8 GHz, and 7.1 GHz.

where d_i is the distance between the feeder phase center and the reflection unit, c is the speed of light, and f is the corresponding operating frequency or the center frequency of the band.

Then, the compensation phase of each unit can be calculated through the above phase compensation formula. According to the above formula, the corresponding compensation phase of the preset reflection angle is calculated in MATLAB. Then, the corresponding ON/OFF state of each unit cell is set in CST. The full-wave electromagnetic simulation is completed in the end. In order to reasonably distribute the ON and OFF states to the unit phase, the unit cell is set to the OFF state when the compensation phase is [0°, 180°]. The unit cell is set to the ON state when the compensation phase is [180°, 360°]. In this way, the direction of the reflected beam is controlled. Similar to binary coding, the ON state is considered as "1" and the OFF state as "0." Based on this mechanism, a 1-bit unit state distribution of 10 × 10 unit cells is obtained by using the feed position d and the target deflection angle.

Figures 6–8 show beams with a range of target deflection angle with their corresponding continuous and discrete phase distributions. The proposed RIS-based antenna can achieve ±40° beam scanning with a gain tolerance of 3 dB. The radiation patterns are basically coincident in different frequencies and the deviation of the main lobe angle is low, indicating that the prototype has stable performance in the full working frequency band. It will not be easily affected by frequency changes. It can be seen from Fig. 9 that the maximum gain is 18.7 dBi, which indicates that the proposed RIS-based antenna has a higher gain.

In order to study the influence of different phase compensation mechanisms on the reconfigurability of RIS-based antenna, the unit cell sets to the OFF state when the compensation phase is [−90°, 90°]. The unit cell sets to the ON state when the compensation phase is [90°, 270°]. Based on this mechanism, another 1-bit unit state distribution of 10 × 10 unit cells is obtained by using the feed position d and the target deflection angle. Taking the target angle of 30° as an example, the phase distribution and the performance of the radiation pattern are shown in Fig. 10. In this mechanism, the RIS-based antenna still can reach the target angle, which means that a stable phase shift is the key to reconfigurable.

As shown in Fig. 11, the two kinds of phase compensation mechanisms have only a little difference in the radiation pattern. To compare the detail directly, the other three performances are shown in Fig. 12. In Fig. 12(a), the amplitude of the main lobe of the latter mechanism is at least 0.6 dB higher than that of the former one. So it can get a better gain when the unit cell is distributed in the latter one. At the same time, the angular width in 3 dB is reduced by up to 4.5°, which means that the RIS-based antenna has better direction performance in the latter one.

Experimental results

The RIS-based antenna is simulated by the CST Microwave Studio. Meanwhile, in order to validate the simulated results, the proposed RIS has been fabricated using the standard printed circuit board technology. Then PIN diodes are soldered on top of the RIS, as shown in Fig. 13(a). Moreover, the bias line network is fabricated on the back of the RIS, as shown in Fig. 13(b).

Based on the previous research [28], the digital control board is designed to control the DC-biasing voltage on each PIN diode to achieve reconfigurability. In this design, the meta-atoms have the same voltage in the same unit cell. So, it only needs to control 100 unit cells to reconfigure 400 PIN diodes. The digital control board design is shown in Fig. 14. The main control chip uses the Single-Chip Microcomputer STM32F103RCT6. The 13 shift registers (74HC595D) are utilized to control all of the unit cells separately. Meanwhile, each LED is connected in series with each unit cell to present the unit cell's status. A Bluetooth module is designed to facilitate the interaction between the digital control board and computers. In the experiment, the RIS is connected to this digital control board to control the phase distribution of RIS. According to the relevant parameters of the control circuit board, the power consumption of this metasurface is about 6.6 W. Referencing the relevant research, the RIS has a range in power consumption from 5.32 W [29], 8 W [30] to 234 W [31]. In this
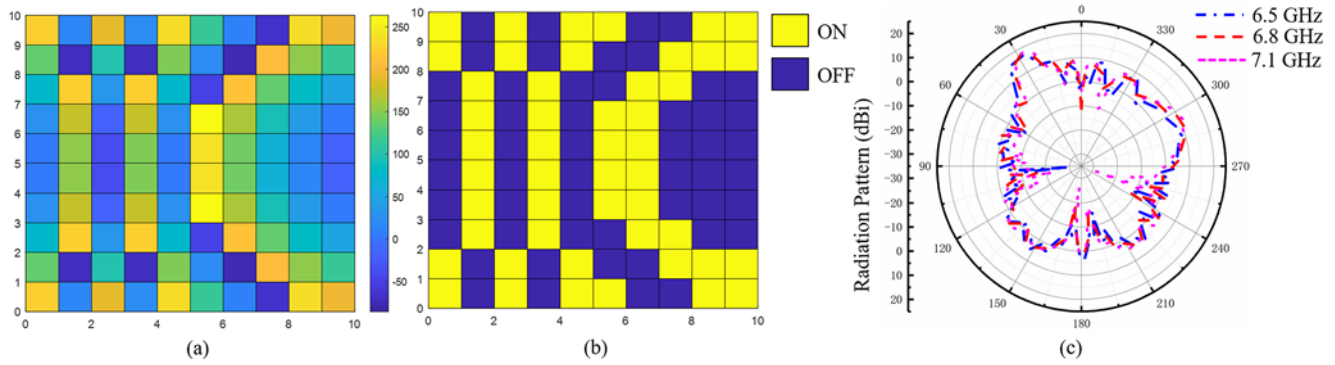
Figure 10. (a) Phase continuous distribution, (b) phase discrete distribution, and (c) simulation pattern at 30°.
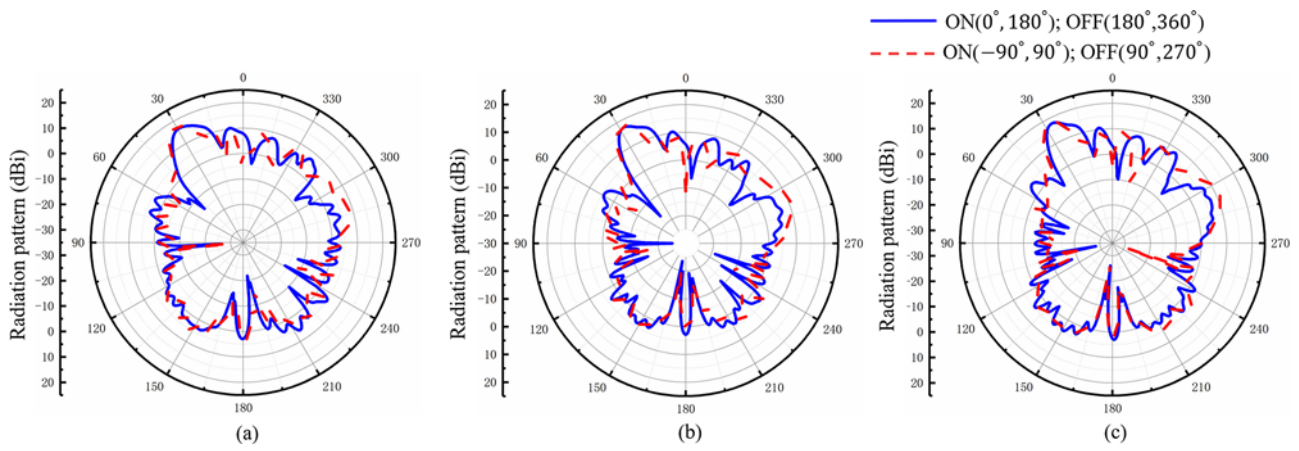

Figure 11. A comparison of the radiation pattern: (a) at 6.5 GHz, (b) at 6.8 GHz, and (c) at 7.1 GHz.
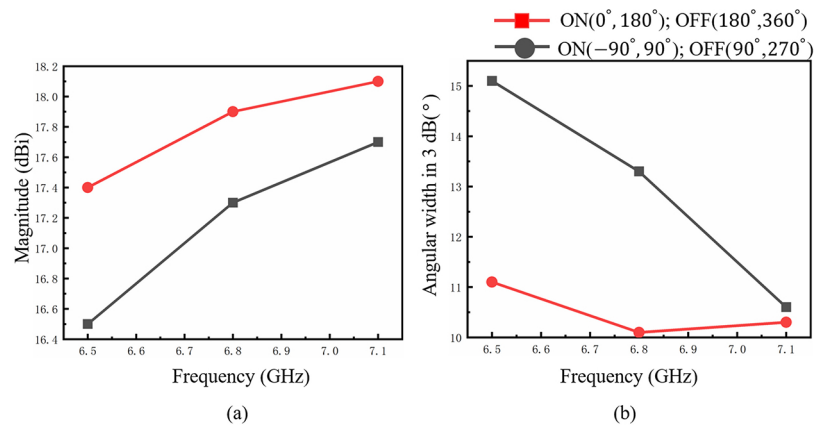

Figure 12. A comparison of the radiation pattern: (a) the main lobe magnitude and (b) the angular width (3 dB).

design, unit combination can simplify the difficulty of control and reduce the number of shift registers and the requirement for high-performance chips on the control board. Although considering the size of the unit cell and the size of the antenna aperture, the number of PIN diodes increases. The power consumption in this design is still maintained at a low level.

Figure 15 shows the measured results with different reflection beam angles at 6.5 GHz, 6.8 GHz, and 7.1 GHz. The measurement results agree well with the simulation ones. The measurement results agree well with the simulation ones, which means

the proposed RIS-based antenna can achieve ±40° beam scanning with a gain tolerance of 3 dB. This also means that a variety of beam distributions can be generated by changing the unit distribution of the two states of the RIS, which indicates that the RIS can quickly create a variety of reflection beams with different modes so as to significantly improve the imaging speed. Due to the impacts of the experimental environment and the extra solder on the surface, there exist certain differences in the measured results. This problem can be solved by improving soldering technology. Meanwhile, the pattern distortion may be cursed by
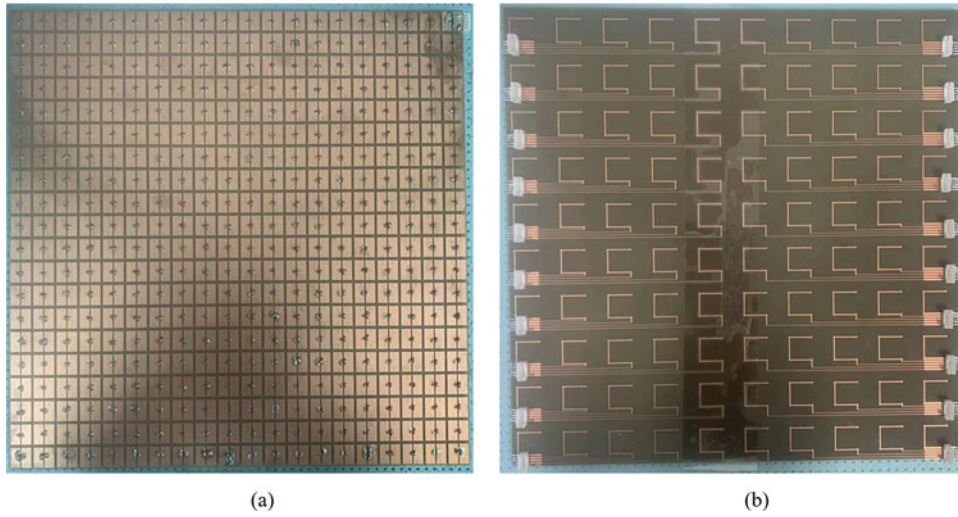
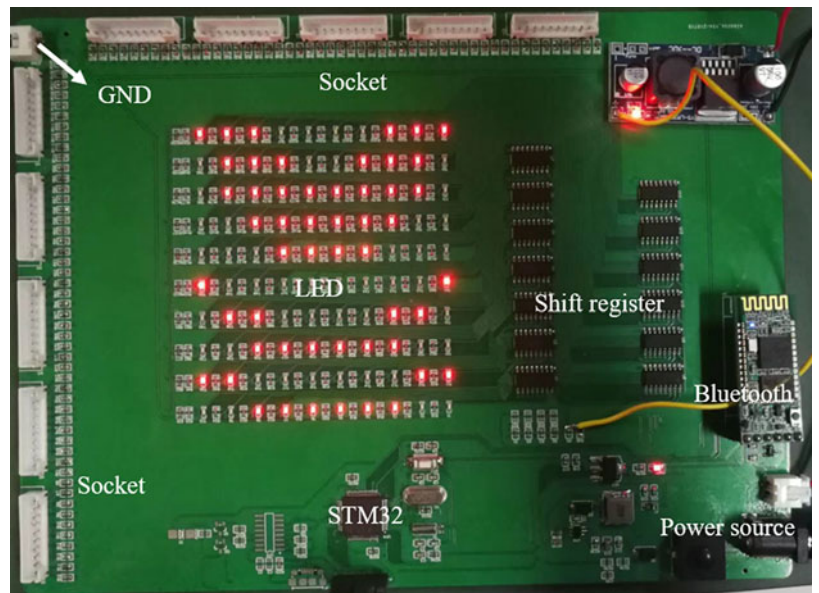**Figure 13.** The photograph of the RIS: (a) top view and (b) back view.

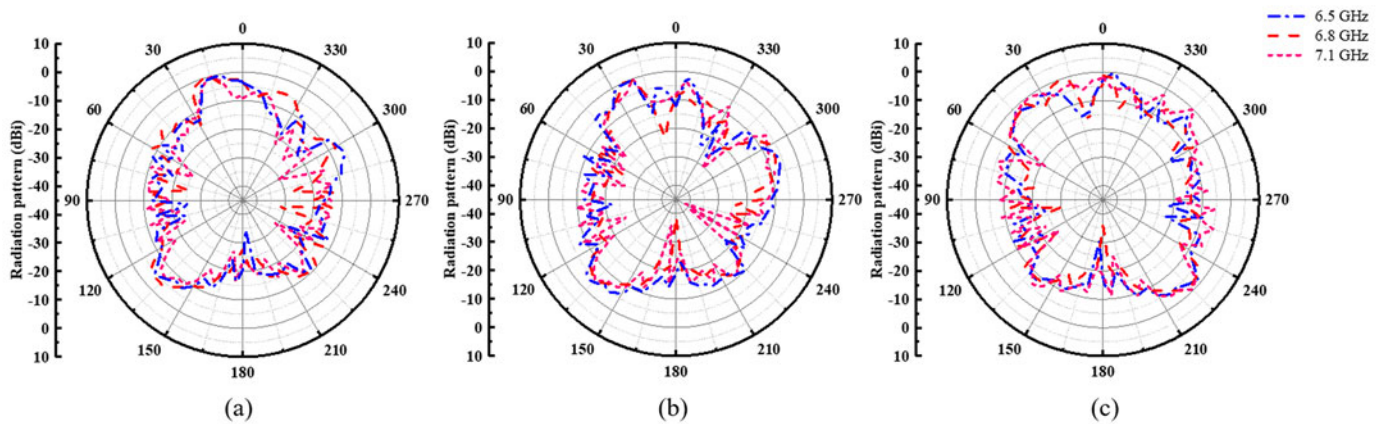**Figure 14.** The photograph of digital control board.

Figure 15. The measured results (a) at 15°, (b) at 30°, and (c) at 40°.

Table 1. Performance comparison of the proposed antenna and similar works

Paper	Size (mm)	Frequency (GHz)	−3 dB beam scanning (°)	Material	Peak gain (dBi)
[28]	725 × 700 (4.83λ × 4.67λ)	2	±40	FR4	16.7
[32]	260.9 × 260.9 (4.62λ × 4.62λ)	5.78−5.84	±40	Rogers RO4003	9.67
[33]	400 × 400 (10λ × 10λ)	7.26−7.82	±45	Rogers RO4003C	25.3
[34]	165 × 165 (15.4 × 15.4λ)	27.5−28.5	±30	Rogers RO4003C	27.22
[35]	360 × 360 (11.7λ × 11.7λ)	6, 9.8	±40	F4B	19.43
This paper	300 × 300 (6.8λ × 6.8λ)	6.425−7.125	±40	FR4	18.7
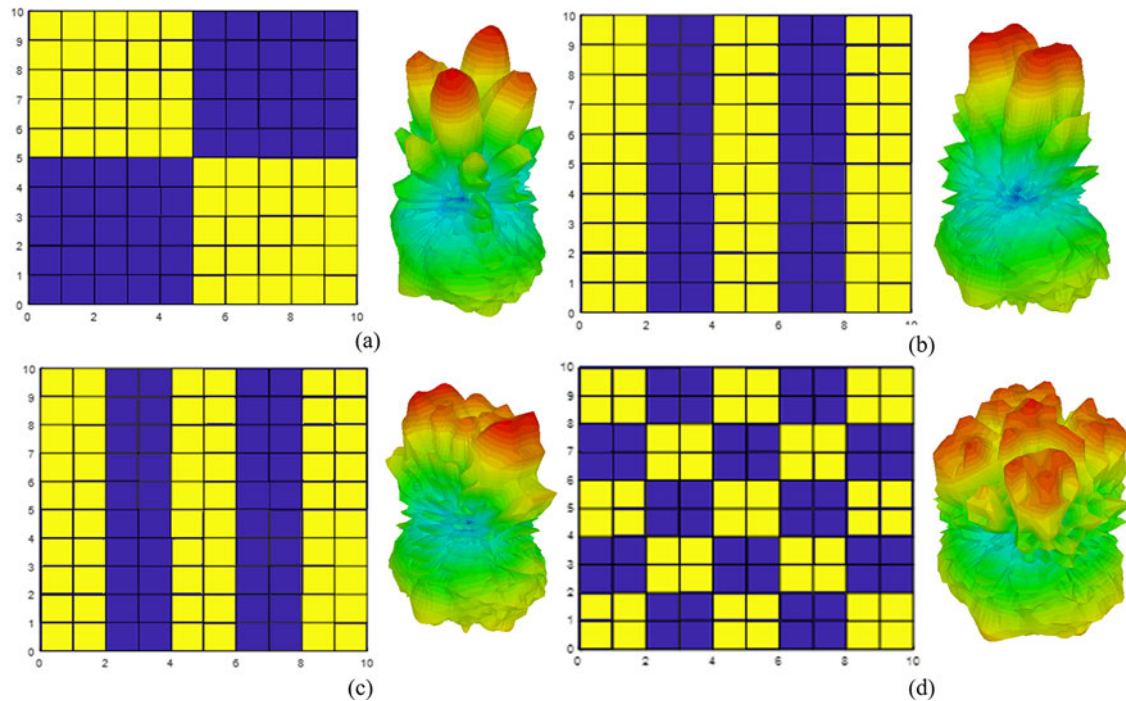
Figure 16. Beamforming: (a) four-beam, (b) two-beam, (c) broad beam, and (d) multi-beam.

the quantization of the phase distribution. Since the measurement environment is not a microwave anechoic chamber and other factors interfere, additional backward radiation power is generated. There is a certain difference between the measurement backward radiation results and the simulation results.

Table 1 shows the performance comparison of this proposed design with the relevant antennas [32–35]. It indicates that this proposed RIS-based antenna has a high peak gain, a small size for the miniaturization requirements, and a large beam scanning area. Especially, compared to the previous research [28], the phase compensation mechanism is optimized in this design, and the optimization of the 2 × 2 meta-atoms as a unit cell is proposed to simplify the bias network. In addition, the frequency selection is to fit the 2023 World Radiocommunication Conference (WRC-23) application background and provide data support for the discussion of WRC2023. In conclusion, the proposed RIS-based antenna has high gain and directivity and flexible reconfigurability, which can be utilized in wireless communication systems and other 5G applications.

RIS of multi-beam

Beam imaging, as an important technology in current and even future wireless communications, helps to achieve dynamic target communication. The realization of multi-beam distribution is helpful for image information transmission in communication. Compared with traditional beam imaging methods, this metamaterial imaging method has the advantages of high speed and high accuracy. Some researchers put forward the metamaterial aperture for calculating imaging. This metamaterial aperture is excited by the waveguide and has frequency diversity, which makes it possible to realize stray beams with a low correlation coefficient in the frequency domain [36]. The use of this aperture imaging not only makes full use of frequency domain resources but also reduces the complexity of beam imaging and can also obtain high-resolution target images. Combining FPGA technology, RIS can also realize automatic beam adjustment through the preset coding in the chip. Moreover, multi-beam distribution is vital for user target tracking and channel reallocation in wireless communication networks.

As shown in Fig. 16, by changing the unit distribution of the two states of the RIS, a variety of beam distributions can be generated, indicating that the RIS can quickly generate a variety of beams with different modes, which greatly improves the imaging speed and the quality of multi-receiver mobile communication. Due to the limitations of the current experimental conditions, the multi-beam radiation is only simulated. Experimental tests and further attempts in this direction will be considered in the future.

Conclusions

A 1-bit 10×10 RIS-based antenna is proposed. This antenna is equipped with a total of 400 PIN diodes, and a digital control chip has been designed to adjust the state of each element according to the target beam angle to achieve reconfigurable functions. Compared with the conventional phased array, this method prevents excessive power consumption and high hardcore costs. In this design, the 2×2 meta-atoms as a unit cell can simplify the bias network and reduce the requirement of the control chip. Meanwhile, it maintains the phase difference and magnitude of the reflection coefficient. This proposed RIS-based antenna can achieve $\pm 40°$ beam scanning with a gain tolerance of 3 dB. Meanwhile, this antenna has a high gain, with a maximum gain of 18.7 dBi. By modifying the phase distribution of the array, the image reconstruction function can be realized, which is suitable for wireless communication systems and microwave imaging systems.

Competing interests. The authors report no conflict of interest.

References

1. **Di Renzo M, Ntontin K, Song J, Danufane FH, Qian X, Lazarakis F, De Rosny J, Phan-Huy D-T, Simeone O and Zhang R** (2020) Reconfigurable intelligent surfaces vs. relaying: Differences, similarities, and performance comparison. *IEEE Open Journal of the Communications Society* **1**, 798–807.
2. **Di Renzo M, Debbah M, Dinh-Thuy P-H, Zappone A, Alouini M-S, Yuen C, Sciancalepore V, Alexandropoulos GC, Hoydis J, Gacanin H, de Rosny J, Bounceur A, Lerosey G and Fink M** (2019) Smart radio environments empowered by reconfigurable AI meta-surfaces: An idea whose time has come. *Eurasip Journal on Wireless Communications and Networking* **2019**, 1–20.
3. **Nayeri P, Yang F and Elsherbeni AZ** (2015) Beam-scanning reflectarray antennas: A technical overview and state of the art. *IEEE Antennas and Propagation Magazine* **57**, 32–47.
4. **Tang W, Chen MZ, Dai JY, Zeng Y, Zhao X, Jin S, Cheng Q and Cui TJ** (2020) Wireless communications with programmable metasurface: New paradigms, opportunities, and challenges on transceiver design. *IEEE Wireless Communications* **27**, 180–187.
5. **Tang W, Li X, Dai JY, Jin S, Zeng Y, Cheng Q and Cui TJ** (2019) Wireless communications with programmable metasurface: Transceiver design and experimental results. *China Communications* **16**, 46–61.
6. **Yang Z, Guo L, Yao C, Zhang Q, Xu Z, Guo M and Wang Z** (2019) Ultrawideband antipodal tapered slot antenna with gradient refractive index metamaterial lens. *IEEE Antennas and Wireless Propagation Letters* **18**, 2741–2745.
7. **Tian HW, Jiang W, Li X, Chen ZP and Cui TJ** (2021) An ultrawideband and high-gain antenna based on 3-D impedance-matching metamaterial lens. *IEEE Transactions on Antennas and Propagation* **69**, 3084–3093.
8. **Xu R and Chen ZN** (2021) A compact beamsteering metasurface lens array antenna with low-cost phased array. *IEEE Transactions on Antennas and Propagation* **69**, 1992–2002.
9. **Wen Q, Wang B-Z and Ding X** (2016) Wide-beam SIW-Slot antenna for wide-angle scanning phased array. *IEEE Antennas and Wireless Propagation Letters* **15**, 1638–1641.
10. **Wang HB and Cheng YJ** (2019) Single-layer dual-band linear-to-circular polarization converter with wide axial ratio bandwidth and different polarization modes. *IEEE Transactions on Antennas and Propagation* **67**, 4296–4301.
11. **Fahad AK, Ruan C, Ali SAKM, Nazir R, Ul Haq T, Ullah S and He W** (2020) Triband ultrathin polarization converter for X/Ku/Ka-Band microwave transmission. *IEEE Microwave and Wireless Components Letters* **30**, 351–354.
12. **Zhao J, Cheng Q, Chen J, Qi MQ, Jiang WX and Cui TJ** (2013) A tunable metamaterial absorber using varactor diodes. *New Journal of Physics* **15**, 043049.
13. **Kim M-S and Kim S-S** (2019) Design and fabrication of 77-GHz radar absorbing materials using frequency-selective surfaces for autonomous vehicles application. *IEEE Microwave and Wireless Components Letters* **29**, 779–782.
14. **Wang Q, Tang X-Z, Zhou D, Du Z and Huang X** (2017) A dual-layer radar absorbing material with fully embedded square-holes frequency selective surface. *IEEE Antennas and Wireless Propagation Letters* **16**, 3200–3203.
15. **Yang H, Yang F, Xu S, Mao Y, Li M, Cao X and Gao J** (2016) A 1-bit 10×10 reconfigurable reflectarray antenna: Design, optimization, and experiment. *IEEE Transactions on Antennas and Propagation* **64**, 2246–2254.
16. **Long M, Jiang W and Gong S** (2017) Wideband RCS reduction using polarization conversion metasurface and partially reflecting surface. *IEEE Antennas and Wireless Propagation Letters* **16**, 2534–2537.
17. **Modi AY, Balanis CA, Birtcher CR and Shaman HN** (2019) New class of RCS-reduction metasurfaces based on scattering cancellation using array theory. *IEEE Transactions on Antennas and Propagation* **67**, 298–308.
18. **Guclu C, Perruisseau-Carrier J and Civi OA** (2012) Proof of concept of a dual-band circularly-polarized RF MEMS beam-switching reflectarray. *IEEE Transactions on Antennas and Propagation* **60**, 5451–5455.
19. **Xu H, Xu S, Yang F and Li M** (2020) Design and experiment of a dual-band 1 bit reconfigurable reflectarray antenna with independent large-angle beam scanning capability. *IEEE Antennas and Wireless Propagation Letters* **19**, 1896–1900.
20. **Clemente A, Diaby F, Di Palma L, Dussopt L and Sauleau R** (2020) Experimental validation of a 2-bit reconfigurable unit-cell for transmit arrays at Ka-Band. *IEEE Access* **8**, 114991–114997.
21. **Vilenskiy AR, Makurin MN, Lee C and Ivashina MV** (2020) Reconfigurable transmitarray with near-field coupling to gap waveguide array antenna for efficient 2-D beam steering. *IEEE Transactions on Antennas and Propagation* **68**, 7854–7865.
22. **Sun S, Jiang W, Gong S and Hong T** (2018) Reconfigurable linear-to-linear polarization conversion metasurface based on PIN Diodes. *IEEE Antennas and Wireless Propagation Letters* **17**, 1722–1726.
23. **Tan X, Sun Z, Jornet JM and Patios D** (2016) IEEE: increasing indoor spectrum sharing capacity using smart reflect-array. In *IEEE International Conference on Communications (ICC)*, Kuala Lumpur, Malaysia.
24. **Dai L, Wang B, Wang M, Yang X, Tan J, Bi S, Xu S, Yang F, Chen Z, Di Renzo M, Chae C-B and Hanzo L** (2020) Reconfigurable intelligent surface-based wireless communications: Antenna design, prototyping, and experimental results. *IEEE Access* **8**, 45913–45923.
25. **WRC-23 Advisory Committee** (2022) Agenda for the 2023 world radiocommunication conference. https://www.fcc.gov/international/wrc-23.
26. **Yu A, Yang F, Elsherbeni AZ, Huang J and Rahmat-Samii Y** (2010) Aperture efficiency analysis of reflectarray antennas. *Microwave and Optical Technology Letters* **52**, 364–372.
27. **Dahri MH, Jamaluddin MH, Seman FC, Abbasi MI, Sallehuddin NF, Ashyap AYI and Kamarudin MR** (2020) Aspects of efficiency enhancement in reflectarrays with analytical investigation and accurate measurement. *Electronics* **9**, 1887.
28. **Wang Z, Zeng W, Zhao X, Guo L and Liu Y** (2022) A 1-bit reconfigurable metasurface antenna for ground penetrating radar application. *International Journal of RF and Microwave Computer-Aided Engineering* **32**, e23189.
29. **Wan X, Xiao Q, Zhang YZ, Li Y, Eisenbeis J, Wang JW, Huang ZA, Liu HX, Zwick T and Cui TJ** (2021) Reconfigurable sum and difference beams based on a binary programmable metasurface. *IEEE Antennas and Wireless Propagation Letters* **20**, 381–385.
30. **Gros J-B, Popov V, Odit MA, Lenets V and Lerosey G** (2021) A reconfigurable intelligent surface at mm-wave based on a binary phase tunable metasurface. *IEEE Open Journal of the Communications Society* **2**, 1055–1064.

31. **Kamoda H, Iwasaki T, Tsumochi J, Kuki T and Hashimoto O** (2011) 60-GHz electronically reconfigurable large reflectarray using single-bit phase shifters. *IEEE Transactions on Antennas and Propagation* **59**, 2524–2531.

32. **Shuai K, Liu C, Yang X and Liu X** (2022) 1-Bit reconfigurable transmitarray with low insertion loss for wireless power transmission. *International Journal of Rf and Microwave Computer-Aided Engineering* **32**, e23354.

33. **Cao A, Chen Z, Fan K, You Y and He C** (2020) Construction of a cost-effective phased array through high-efficiency transmissive programmable metasurface. *Frontiers in Physics* **8**, 589334.

34. **Xue C, He Q, Li T and Gao X** (2022) 1-Bit dual-polarized ultrathin lens antennas based on Huygens' metasurface. *Frontiers in Materials* **9**, 508.

35. **Zhang N, Chen K, Zheng Y, Hu Q, Qu K, Zhao J, Wang J and Feng Y** (2020) Programmable coding metasurface for dual-band independent real-time beam control. *IEEE Journal on Emerging and Selected Topics in Circuits and Systems* **10**, 20–28.

36. **Li L, Cui TJ, Ji W, Liu S, Ding J, Wan X, Li YB, Jiang M, Qiu C-W and Zhang S** (2017) Electromagnetic reprogrammable coding-metasurface holograms. *Nature Communications* **8**, 197.

Yajun Zhou was born in Jinhua City, Zhejiang Province, China, in 1996. She received her B.E. degree in communication engineering from Kunming University of Science and Technology, China, in 2018. Currently, she is a master student at the University of Geosciences, Beijing. Her main research interest includes reconfigurable intelligent metasurface and reconfigurable reflectarray antenna.

Lianfeng Chen was born in Yichang City, Hubei Province, China, in 1999. She received her B.E. degree in measurement and control technology and instrument in 2021. She is now a graduate student of the China University of Geosciences, Beijing. Her main research interest in reconfigurable intelligence surface.

Qifei Zhang was born in Anqing City, Anhui Province, China, in 2000. He received a bachelor's degree in civil engineering in 2017. He is now studying at the China University of Geosciences, Beijing. He is now a graduate student of the China University of Geosciences, Beijing. His main research interests are ground penetrating radar, synthetic aperture, and two-dimensional imaging.

Hao Wang was born in Erdos City, Inner Mongolia autonomous region, China, in 1999. She received her B.E. degree from China University of Geosciences, Beijing, in 2021. She is now a graduate of the China University of Geosciences, Beijing. Her main research interest is antenna optimization.

Linyan Guo was born in Yangcheng City, Shanxi Province, China, in 1989. She received her B.E. degree in electronic information science and technology in 2011. She also received the M.E. degree in electromagnetic field and microwave technology in 2013 and Ph.D. degree in radio physics from Central China Normal University, Wuhan, China, in 2016, respectively. Currently, she is an associate professor of the China University of Geosciences, Beijing. Her main research interest includes the theory and application of metamaterials, analysis and synthesis of antennas, and ground penetrating radar.